PNAS Nexus, 2023, 2, 1–13
https://doi.org/10.1093/pnasnexus/pgad079
Advance access publication 18 March 2023
Research Report

Acinetobacter baumannii adaptation to the host pH microenvironment is mediated by allelic variation in a single residue of BauA protein

Tao Li[a,1], Deyan Luo[a,1], Nianzhi Ning[a,1], Xiong Liu[a,1], Fanghong Chen[a,1], Liangyan Zhang[a], Chunmei Bao[b], Zhan Li[a], Deyu Li[a], Hongjing Gu[a], Fen Qu[b], Xiaolan Yang[a], Yanyu Huang[a], Boan Li[b] and Hui Wang[a,*]

[a]State Key Laboratory of Pathogen and Biosecurity, Beijing Institute of Microbiology and Epidemiology, No. 20 Dongdajie Street, Fengtai District, Beijing 100071, China
[b]Department of Clinical Laboratory, The Fifth Medical Center of PLA General Hospital, No. 100 West Fourth Ring Road, Beijing 100039, China
*To whom correspondence should be addressed: Email: geno0109@vip.sina.com
[1]T.L., D.L., N.N., X.L., and F.C. contributed equally to this work.
Edited By: Marenda Wilson-Pham

Abstract

Acinetobacter baumannii has been listed as one of the most critical pathogens in nosocomial infections; however, the key genes and mechanisms to adapt to the host microenvironment lack in-depth understanding. In this study, a total of 76 isolates (from 8 to 12 isolates per patient, spanning 128 to 188 days) were longitudinally collected from eight patients to investigate the within-host evolution of *A. baumannii*. A total of 70 within-host mutations were identified, 80% of which were nonsynonymous, indicating the important role of positive selection. Several evolutionary strategies of *A. baumannii* to increase its potential to adapt to the host microenvironment were identified, including hypermutation and recombination. Six genes were mutated in isolates from two or more patients, including two TonB-dependent receptor genes (*bauA* and *BJAB07104_RS00665*). In particular, the siderophore receptor gene *bauA* was mutated in multiple isolates from four patients with three MLST types, and all mutations were at amino acid 391 in ligand-binding sites. With 391T or 391A, BauA was more strongly bound to siderophores, which promoted the iron-absorption activity of *A. baumannii* at acidic or neutral pH, respectively. Through the A/T mutation at site 391 of BauA, *A. baumannii* displayed two reversible phases to adapt to distinct pH microenvironments. In conclusion, we demonstrated the comprehensive within-host evolutionary dynamics of *A. baumannii*, and discovered a key mutation of BauA site 391 as a genetic switch to adapt to different pH values, which may represent a model in the pathogen evolutionary adaption of the host microenvironment.

Keywords: *Acinetobacter baumannii*, within-host evolution, adaptive mutation, iron absorption, siderophore receptor

Significance Statement

Acinetobacter baumannii has been listed as one of the most critical pathogens in nosocomial infections, which has the ability to persist in tissues and cause chronic infection. In this study, we present a longitudinal analysis of sputum samples from eight patients suffering from chronic *A. baumannii* infections, to examine within-host evolutionary dynamics and key adaptive genes. This analysis enabled several mechanisms of evolution and host adaptation for *A. baumannii* to be uncovered including hypermutation and recombination. Importantly, we discovered an adaptive site 391 of the siderophorer receptor BauA as an important regulator for *A. baumannii* to adapt to different pH levels, which depicts a model for bacteria adaptation to a constantly changing host microenvironment.

Introduction

Acinetobacter baumannii is an important opportunistic pathogen that can cause various infections, such as ventilator-associated pneumonia, bloodstream infections, skin and soft-tissue infections, wound infections, and urinary tract infections (1). During the last three decades, *A. baumannii* has become a leading cause of nosocomial infections (2), primarily due to the rapid spread of multidrug-resistant (MDR) *A. baumannii* strains in hospitals (3). MDR *A. baumannii* has been listed by the World Health Organization as one of the most critical pathogens in hospitals; in particular, few treatment options are available for patients infected with *A. baumannii* strains, which poses a serious problem for healthcare facilities.

Acinetobacter baumannii can persist in tissues, which leads to chronic infection. It is believed that two attributes, drug resistance and adaptation to the host environment, have enabled *A. baumannii* to thrive in patients for a long periods (1). In addition

Competing Interest: The authors declare no competing interest.
Received: August 6, 2022. **Revised:** February 20, 2023. **Accepted:** February 28, 2023
© The Author(s) 2023. Published by Oxford University Press on behalf of National Academy of Sciences. This is an Open Access article distributed under the terms of the Creative Commons Attribution-NonCommercial-NoDerivs licence (https://creativecommons.org/licenses/by-nc-nd/4.0/), which permits non-commercial reproduction and distribution of the work, in any medium, provided the original work is not altered or transformed in any way, and that the work is properly cited. For commercial re-use, please contact journals.permissions@oup.com

to antibiotics, *A. baumannii* must also overcome various challenges in the host, such as a lack of nutrient sources, constant changes in the microenvironment (e.g. pH), and immune response clearance. Bacteria have developed many strategies to adapt to diverse and ever-changing conditions. These mechanisms include multidimensional modifications within their genomes, such as point mutations and recombination.

Whole-genome sequencing (WGS) provides a powerful tool for pathogen genome analysis (4–6). It has widely been used to investigate the epidemiology of MDR *A. baumannii* infection outbreaks in hospitals (7) and academic burn centers (8), population and genome dynamics during colonization and infection (9, 10), the dissemination and variation of MDR *A. baumannii* strains (11), and the development of drug resistance (12, 13). However, due to the lack of isolates from chronically infected patients, the evolutionary dynamics and genetic basis for prolonged survival of *A. baumannii* in the host environment have rarely been studied.

In this study, we investigated the clinical course of eight inpatients with MDR *A. baumannii* chronic infections in the Fifth Medical Center of PLA General Hospital in Beijing, China. A total of 76 isolates sampled from the sputum of each patient were longitudinally collected. Through WGS and comparative analysis of all available strains, we sought to uncover the evolutionary dynamics of *A. baumannii* and discover the key adaptive genes and mechanisms in chronic persistent infection.

Results

Longitudinal collection and microevolutionary analysis of the isolates from patients

To develop a comprehensive genomic view of *A. baumannii* evolution within the host, we selected and collected isolates sampled from chronic inpatients in China. The selection criteria for the patients were as follows: availability of numerous longitudinally sampled isolates (>8 isolates); relatively similar isolated time intervals; and long isolate time spans (>120 days). Finally, we longitudinally collected 76 *A. baumannii* isolates sampled from eight patients (Table S1) who had long intensive care unit (ICU) stays and multiple clinical symptoms, including pneumonia. The number of isolates per patient was in the range of 8–12 during a time span of 128–188 days between the first and the last isolation (Fig. 1A, Table S2). The resistance profile of the strains was determined using standard antimicrobial susceptibility tests (Table S3). The results showed that all of the isolates, except for the strain P7_T05, were resistant to more than three classes of antibiotics, including commonly used drugs such as cefoperazone/sulbactam (SCP), ciprofloxacin (CIP), and meropenem (MEM); these 75 strains were considered MDR *A. baumannii*.

To identify genomic changes that accumulate during longitudinal infection, the whole genomes of 76 isolates were sequenced by an Illumina HiSeq 2000 platform to >200-fold coverage. A core phylogeny tree was constructed using kSNP3 software (14). A total of 58,558 single-nucleotide polymorphisms (SNPs) were identified, which were used to build a phylogenetic tree. All strains were categorized into five major clades (clades A–E), except for the strain P7_T05 (Fig. 1B, Table S2). In addition, we performed multilocus sequence typing (MLST) analysis for these 76 strains in accordance with the Oxford MLST typing system (15). Four MLSTs were found, except in the strain P7_T05 (ST819), which was in agreement with the clade analysis results based on whole-genome SNPs (Fig. 1B).

Then, we carefully compared the genomes of the isolates from each patient to infer the microevolution of MDR *A. baumannii* in each patient. The three temporary acquisition strains (P7_T05, P8_T06, and P8_T07) were excluded from the following analysis. Positions differing from the first isolate (T01) in each patient were considered mutation sites, and the SNPs within each patient were identified. A total of 78 mutation sites were found in these eight patients, and all of the mutations were annotated in accordance with the reference genome BJAB07104 (accession number: NC_021726). All of the mutations were verified by PCR amplification and Sanger sequencing. Eight mutations in the isolates from patient P1 were clustered in the 44 bp genome sequence from site 1653441 to site 1653484 (Fig. S1), which was identified as a recombination event using Gubbins (16). The recombination event was identified in the gene *BJAB07104_RS08095*, which encodes a putative secretion-activating protein (Fig. S1). Although recombination has already been reported as a common phenotype in *A. baumannii* (17), to the best of our knowledge this is the first time that it has been described in the evolution within the host. The remaining 70 SNPs included 56 nonsynonymous mutations (NS), eight synonymous mutations (S), and six mutations in noncoding regions (NC). Hence, there was a high proportion of NS relative to S during within-host evolution [NS/(NS + S), 0.91 ± 0.09]. The mutations were significantly more common in the coding regions (Table S4, $P = 0.02$), and there were significantly more nonsynonymous than synonymous mutations ($P < 0.01$), indicating the dominance of positive selection during the within-host evolution of *A. baumannii*.

The rate of diversification was calculated for each patient using the mean pairwise SNP distance (18); a large variation was found among the isolates from the eight patients (8.8 ± 7.1 SNPs genome^{-1} y^{-1}; Fig. 1C). In particular, P4, P6, P7, and P8 were infected by a common clade D *A. baumannii* strain; however, the rate of diversification in patient P7 (1.3 SNPs genome^{-1} y^{-1}) was much lower than that in the other three patients (P4: 6.8; P6: 6.5; P8: 4.7 SNPs genome^{-1} y^{-1}). The results showed that the host microenvironment may be an important factor contributing to the diversification rate of *A. baumannii*. In one patient (patient P2), the diversification rate (27.5 SNPs genome^{-1} y^{-1}) was significantly higher than that in the isolates from other patients (Fig. 1C, $P < 0.01$, Grubbs' test for outliers). Then, we found that all of the isolates from patient P2 contained a single nonsynonymous mutation P118S in the DNA repair relative protein MutS (Fig. S2). Mutation site 118 is at a conserved position in MutS domain I in MutS (Fig. S3), and its defects are known to cause excess mutations (19). The results suggested the presence of hypermutation in the isolates from patient P2. Although hypermutation is a common phenotype in many pathogens, such as *Pseudomonas aeruginosa* in cystic fibrosis patients, and it is hypothesized to accelerate the evolution of antibiotic resistance, it has not previously been described in *A. baumannii*.

The within-host mutation events of the isogenetic strains across multiple patients

Microevolutionary analysis of pathogen genomes (20) was applied to investigate transmission. As shown in the results of the phylogenetic analysis (Fig. 1B), there were 33 strains from four patients, and they all belonged to the same clade D. All these four patients were in a respiratory ward, and there was an overlap in their hospitalization time, which might indicate putative transmissions or the infection of a common ancestry strain in the hospital environment (5) (Fig. 1D). By tracking the mutations detected in the

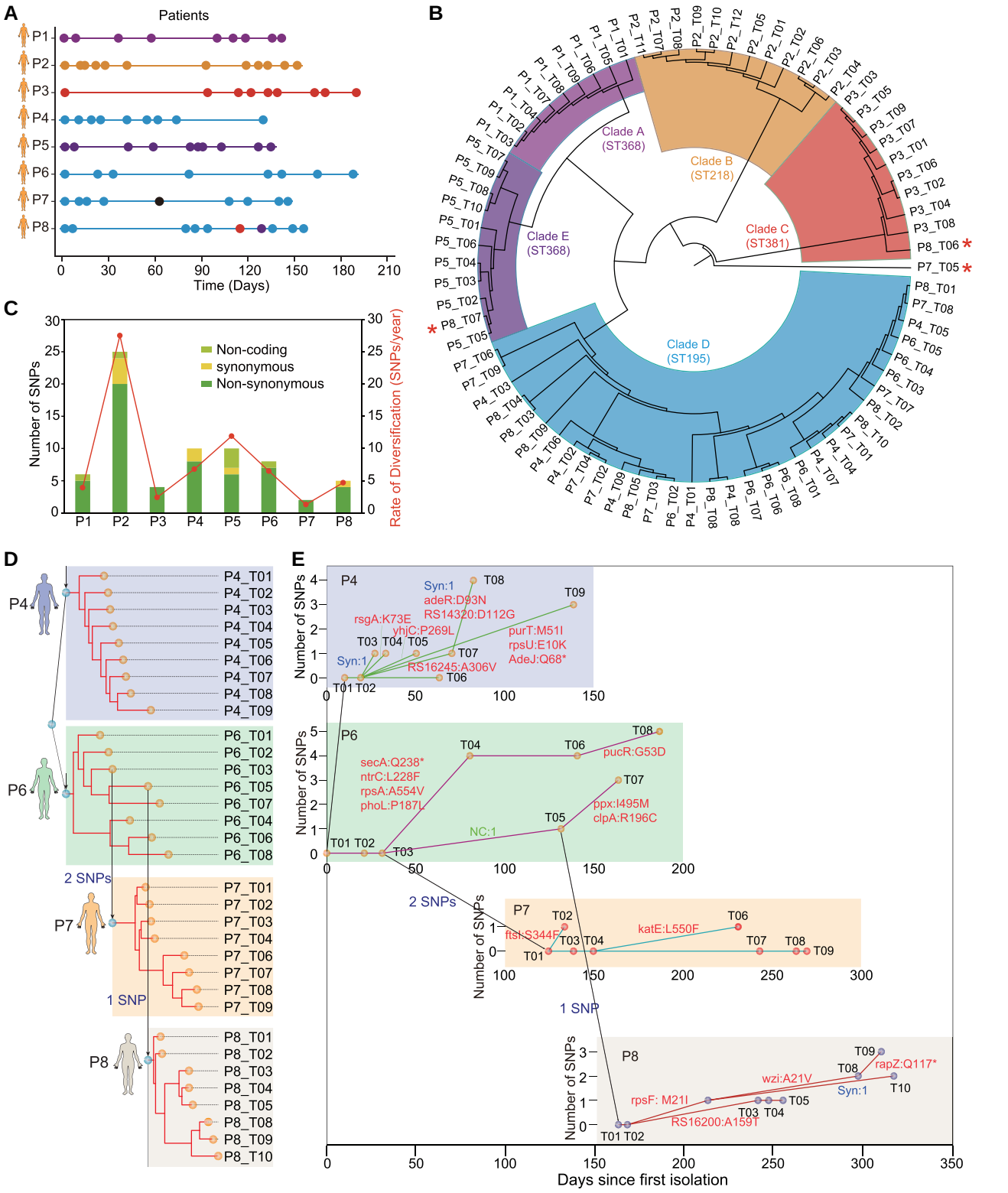

Fig. 1. Longitudinal collection and evolutionary analysis of *Acinetobacter baumannii* isolates in patients. A) The isolated dates of each strain from eight patients. The segments represent the isolation time of each strain; each point represents a strain; the color of each point represents clade designation. P7_T05, P8_T06, and P8_T07 were in different clade with other strains of patient P7 or P8. B) Phylogenetic structure of 76 MDR *A. baumannii* strains. SNPs were identified using kSNP3 (version 3.021). kSNP3 parsimony tree, which is a consensus of up to 100 equally parsimonious trees, was constructed using 58,558 SNPs that were present in 80% of the strains. Five major clades A–E and the corresponding four MLST types were found. Strain P7_T05 was an exception, which did not belong to any clade. C) Number of SNPs and rate of diversification in each patient. Left: each bar represents the number of SNPs found in each patient; three types of mutations are indicated by different colors. Right: eachpoint represents the rate of diversification calculated in each patient. D) Maximum-likelihood phylogenetic tree inferred from SNP alignment of the isolates in clade D. The transmission events were reconstructed. Patients P4 and P6 had been infected by a common clade D, and infection of patients P7 and P8 stemmed from P6 in the same ward. E) Time-scaled minimum spanning trees of the isolates from four patients. The annotation of SNPs is labeled on branches. Four patients are indicated by four colors, and the date of the first isolation in these four patients is the origin point of the x-axis. The numbers of SNPs compared with the first isolate are shown on the y-axis.

longitudinally collected genomes from each of the patients, we constructed the complete landscapes of the sequence of mutation events from the first to the last isolate in different patients (Fig. 1E). The clade D strains had distinct mutation genes, sites, and dominant clone types among the four patients (Fig. 1E). In patient P4, the strains evolved into a diverse community, including multiple clone types with different mutations. In patient P6, two dominant clone types appeared simultaneously in the strains, which may reflect two distinct host microenvironments in different infection sites. In contrast, different dominant clone types appeared successively in the strains from P8 to adapt to the changes in the host microenvironment. In the strains from P7, the initial strain was continuously the dominant clone type. All these findings further confirm the crucial role of the host microenvironment in the evolutionary within-patient dynamics of *A. baumannii*.

Parallel mutated genes involved in the within-host evolution of *A. baumannii*

To observe the within-host evolution of *A. baumannii* at the gene levels, we sought to identify genes that showed parallel evolution in different hosts. Finally, a total of six genes (*bauA*, *wzc*, *ntrC*, *AdeJ*, *BJAB07104_RS00665*, and *BJAB07104_RS16200*) were mutated in multiple patients or MLST types (Fig. 2A). These six genes were more frequently mutated than what would be expected under random conditions ($P < 0.01$), which suggests that parallel mutations in these six genes are the result of positive selection undergoing adaptive evolution. The gene *wzc* (also referred as *ptk*) was identified with three nonsynonymous mutations (ST368 in P1: A540G, ST381 in P3: L567F, G667D; Fig. 2B), encodes a putative protein tyrosine kinase, and is required for capsule formation (21). All of the mutations were located in a conserved region of Wzc (pfam10609: ParA domain; Fig. 2B). The results showed that none of the three mutations (G667D, L567F and A540G) affected the amount of the capsule (Fig. S4A), but two mutations (G667D and A540G) significantly changed the capsule diameters (Fig. S4B). The mutation G667D, which was also identified in a previous report (22), significantly increased the capsule diameters ($P < 0.01$). In contrast, the mutation A540G significantly decreased the capsule diameters ($P < 0.01$). Capsule formation is important for immune escape of pathogens during infection and is a major virulence factor in *A. baumannii* infection (23, 24). These adaptive mutations in the Wzc protein might bring some advantage for the strain to escape the host immune response. AdeJ is a part of a three-component RND efflux system AdeIJK in *A. baumannii*, which contributes to the resistance to multiple antibiotics (25). Two mutations were identified in the *adeJ* gene, and both of them resulted in a premature stop codon and gene inactivation (ST218 in P2:W13*, ST195 in P4:Q68*). These two mutations were only found in a single isolate and were not identified in the subsequent isolates in two patients, indicating that these two mutations served for temporary adaptation to a special host environment. A transcriptional regulator gene *ntrC* was mutated in two clades (ST218 in P2: L228F, ST195 in P6: L187I). NtrC is a part of a two-component system, which has been reported to be an important regulator during stress response (26). Thus, the nonsynonymous mutation in NtrC may modulate the expression of regulated genes, which is helpful for the survival of *A. baumannii* in the host. The gene *BJAB07104_RS16200* that codes a protein with a domain of LPS biosynthesis glycosyl-transferase was mutated in multiple isolates from two patients (ST368 in P1:S8R, ST195 in P8: A159T). In particular, two genes (*BJAB07104_RS00665*, *bauA*) encoding the domain of TonB-dependent receptor (pfam00593: TonB_dep_Rec) were mutated in the isolates from different patients. The gene *BJAB07104_RS00665*, which encodes the putative receptor for an unknown substrate, was mutated in the isolates of patients P2 and P4 (ST218 in P2:D111A, ST195 in P4: synonymous mutation in site 643; Fig. 2B). The gene *bauA* was mutated in the isolates from four patients with three MLST types (ST368 in P1 and P5: T391A, ST218 in P2: A391T, ST381 in P3: A391T; Fig. 3A), and it encodes an acinetobactin (or preacinetobactin) outer membrane receptor protein (27). The mutation (A391T) has also been identified in *A. baumannii* isolates in previous research (22). They were all mutated at the same amino acid position (site 391) in a conserved domain of TonB_dep_Rec (pfam00593; Fig. 3A). Interestingly, the mutations both A391T and T391A were found in multiple isolates from four patients (P1, P2, P3, and P5; Fig. 3A). The results showed that site 391 of BauA was involved in the within-host evolution, which may be a key mutation site for the host adaptation of *A. baumannii*.

BauA-391 mutation alters the pH-related iron-absorption activity of *A. baumannii*

BauA is a multiple transmembrane protein receptor for preacinetobactin (and acinetobactin), which is a major siderophore utilized by the human pathogen *A. baumannii* (28). In addition, 2D and 3D topology models of the BauA protein showed that site 391 is located in the ligand-binding sites of BauA (364–392 amino acids, Fig. 3B), which is in the fifth loop of the extracellular region (Fig. S5). These data suggested that BauA's T391A or A391T mutation may affect the iron acquisition activity of *A. baumannii*. *Acinetobacter baumannii* is capable of growing over a wide pH range, with most sites of infection being acidic (29); thus, the activity of siderophore-mediated iron acquisition (Fig. 3C) was identified at pH from 5.8 to 7.2. Interestingly, the levels of $^{55}Fe^{3+}$ uptake of the clinical isolates from P2 or P5 were significantly different in a neutral (pH 7.2) or acidic environment (pH 5.8 or 6.5; Fig. 3D, $P < 0.01$). The six clinical isolates (from P2-T01 to P2-T06) with BauA-391A acquired more $^{55}Fe^{3+}$ at pH 7.2; in contrast, the other six clinical isolates (from P2-T07 to P2-T12) with BauA-391T acquired significantly more $^{55}Fe^{3+}$ at pH 5.8 or 6.5 (Figure 3D, left panel). Similar results were also detected in the 10 clinical isolates from P5 (P5-T01 to P5-T10, Fig. 3D, right panel). Then, we further confirmed the results with the same genetic strains. The single amino acid mutant of the BauA 391 site (A391T, named 391T) or the deleted mutant of the *bauA* gene (named Δ*bauA*) of strain P5_T08 (named 391A) was generated using a suicide plasmid recombination system (30), and the activity of iron acquisition was detected and compared (Fig. 3E). The levels of $^{55}Fe^{3+}$ uptake of the strain with 391A were significantly higher than those in the strain with 391T at pH 7.2 ($P < 0.01$); in contrast, they were significantly lower at an acidic pH (at pH 5.8 or 6.5, $P < 0.01$). The activity of Δ*bauA* was significantly reduced compared with the two mutants at both neutral and acidic pH. The results demonstrated that the mutation between 391A and 391T in BauA promoted the iron-absorption activity of *A. baumannii* at different pH values to adapt to an iron-deficient environment.

The mutations 391A and 391T enhance BauA's binding ability to siderophore at acidic or neutral pH

To uncover the molecular basis of the activity of BauA site 391, two types of BauA protein with 391T and 391A were expressed and purified, and the interactions between BauA and siderophore-Fe^{3+} (2:1) at different pH values were identified by

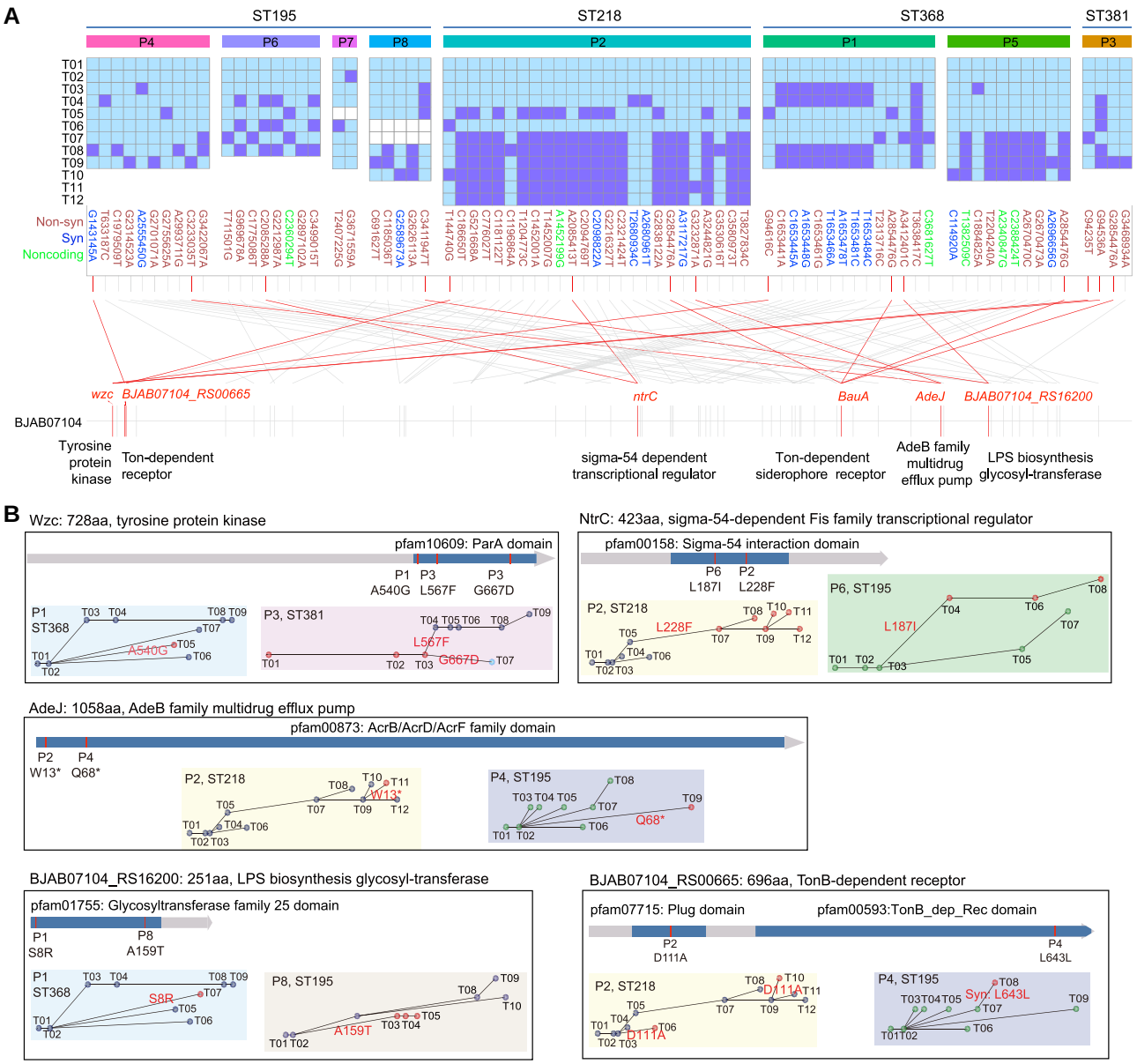

Fig. 2. Parallel mutated genes involved in within-host evolution of *Acinetobacter baumannii*. A) SNPs pattern of each patient. Top: Eight patients ordered according to their MLST types. A total of 10, 8, 2, 5, 25, 14, 10, and 4 SNPs were found in patients P4, P6, P7, P8, P2, P1, P5, and P3, respectively. The dark squares represent mutations compared with the first isolate in each patient, and the light squares represent no mutations. Left margin: isolated time of each patient, P4 (T01–T09), P6 (T01–T08), P7 (T01–T08), P8 (T01–T8), P2 (T01–T12), P1 (T01–T09), P5 (T01–T10), and P3 (T01–T09). Three types of mutation are indicated by different colors. Bottom: SNP position in BJAB07104 genome and genes mutated in different patients are indicated. B) Distribution of the mutants of five proteins (Wzc, AdeJ, NtrC, BJAB07104_RS16200, and BJAB07104_RS00665), which were mutated in multiple patients or MLST types. The mutants are marked with different colors in the time-scaled minimum spanning trees.

isothermal titration calorimetry (ITC; Fig. 4A). The results showed that the combination of BauA and siderophore-Fe^{3+} was greatly influenced by pH. For example, at pH 7.2, the interaction between BauA and the siderophore-Fe^{3+} complex was an exothermic reaction; in contrast, the binding reaction was endothermic at pH 5.8 or 6.5 (Fig. 4A). More importantly, the mutations between 391A and 391T remarkably enhanced the affinity of BauA and siderophore-Fe^{3+} at acidic or neutral pH, respectively. The binding affinity of BauA-391A was higher than that of BauA-391T at pH 7.2 (Kd: 2.47E-6 vs. 2.67E-5) and lower than that at acidic pH (Kd: 2.14E-7 or 4.06E-6 vs. 3.78E-5 or 1.30E-5 at pH 5.8 or 6.5). These results revealed that through the opposite mutations at BauA-391, *A. baumannii* was able to increase its own iron levels in response to the challenges of pH change. When environmental pH changed from neutral to acidic, the binding affinity between siderophore-Fe^{3+} and BauA-391A gradually increased, thereby improving the iron-absorption capacity and intracellular iron concentration (Fig. 4B). In contrast, when pH values changed inversely, through a point mutation from 391A to 391T, *A. baumannii* maintained strong siderophore-Fe^{3+} binding ability and acquired more exogenous iron ions.

BauA-391T/A variants are dominant in distinct pH microenvironments

To address the character of BauA-391T/A variation, we investigated the sequences of protein BauA from different strains of

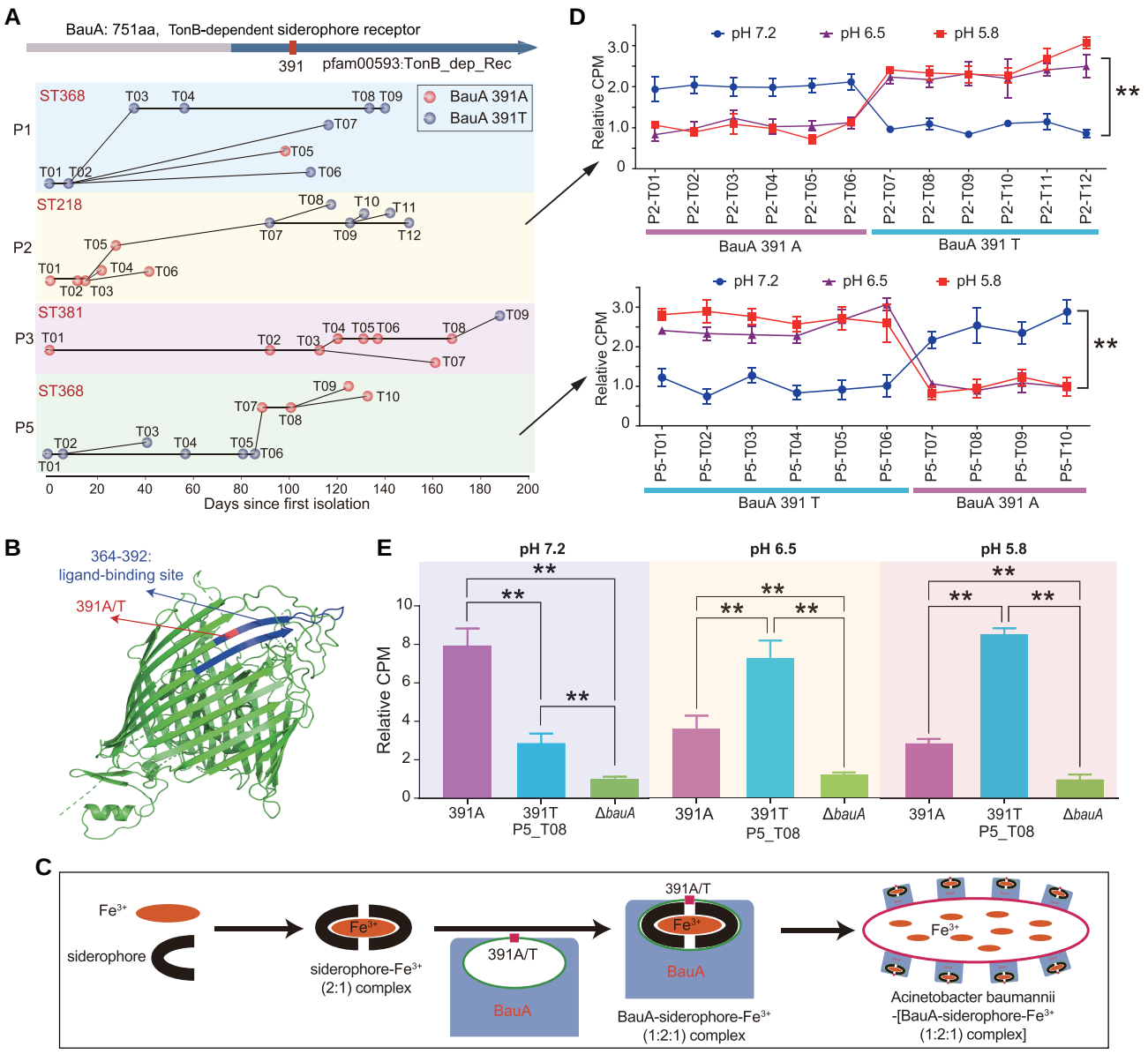

Fig. 3. BauA-391 mutation alters the pH-related iron-absorption activity of *Acinetobacter baumannii*. A) Time-scaled minimum spanning trees of the isolates from four patients with gene *bauA* mutation. The mutants in site 391 were found in three MLST type strains from four patients: A391T in ST218 in patient P2, T391A in ST368 in patients P1 and P5, A391T in ST381 in patient P3. The mutants 391A or 391T are marked with different colors. B) The 3D topology model of BauA protein. Site 391A is located in one of the extracellular loops, which is a part of the ligand-binding site. C) The model of siderophore-mediated iron acquisition in *A. baumannii*. The siderophore can chelate Fe^{3+} at a ratio of 2:1, and the complex can be recognized and transported by the outer membrane transporter BauA in *A. baumannii*. D) In vitro uptake of $^{55}Fe^{3+}$-siderophore with different clinical isolates at different pH values. $^{55}Fe^{3+}$-siderophore (1:2) solution was added to iron-starved clinical strains from patients P2 and P5 at pH 7.2, 6.5, or 5.8. The radioactivity levels of the strains were detected and compared. The data shown depict the average of six independent experiments. E) In vitro iron uptake assays. $^{55}Fe^{3+}$-siderophore (1:2) solution was added to iron-starved strains, including the mutants 391A, 391T, and Δ*bauA* of *A. baumannii* strain P5_T08, at pH 5.8, 6.5, or 7.2. The data shown depict the average of six independent experiments. **$P < 0.01$.

A. baumannii in the NCBI database (Fig. S6). The BauA proteins of *A. baumannii* are divided into three clades based on sequence similarity (Fig. S6A and S6E), and the BauA proteins of each clade are encoded by the strains of different MLST types (Fig. S6B–D). Among the three clades, clade I is with the largest number of strains and protein sequences (Fig. S6A and S6E). Many MLST types (e.g. ST208, ST195) that have recently been reported to be prevalent in MDR *A. baumannii* belong to clade I (Fig. S6C) (31–33). The BauA proteins of 75 MDR strains in this study belong to clade I, and the sequence homology with clade II or III is 69 to 70% or 58 to 59%, respectively (Fig. S6F). Especially, site 391 is the only high-frequency mutation site in BauA proteins of clade I (Fig. S6G). Among the 12,133 sequences in clade I, the frequencies of two amino acid residues (T and A) at BauA 391 site are 56.5 and 40.2%, respectively (Fig. S6H). The high proportions of these two amino acids in nature further emphasize the importance of this mutation site in the environmental persistence of the clade I strains of *A. baumannii*.

To better understand the physiological significance of the mutation between 391A and 391T, the growth and infection levels of the two mutants were examined at different pH values. The growth curves of *A. baumannii* with different mutations were

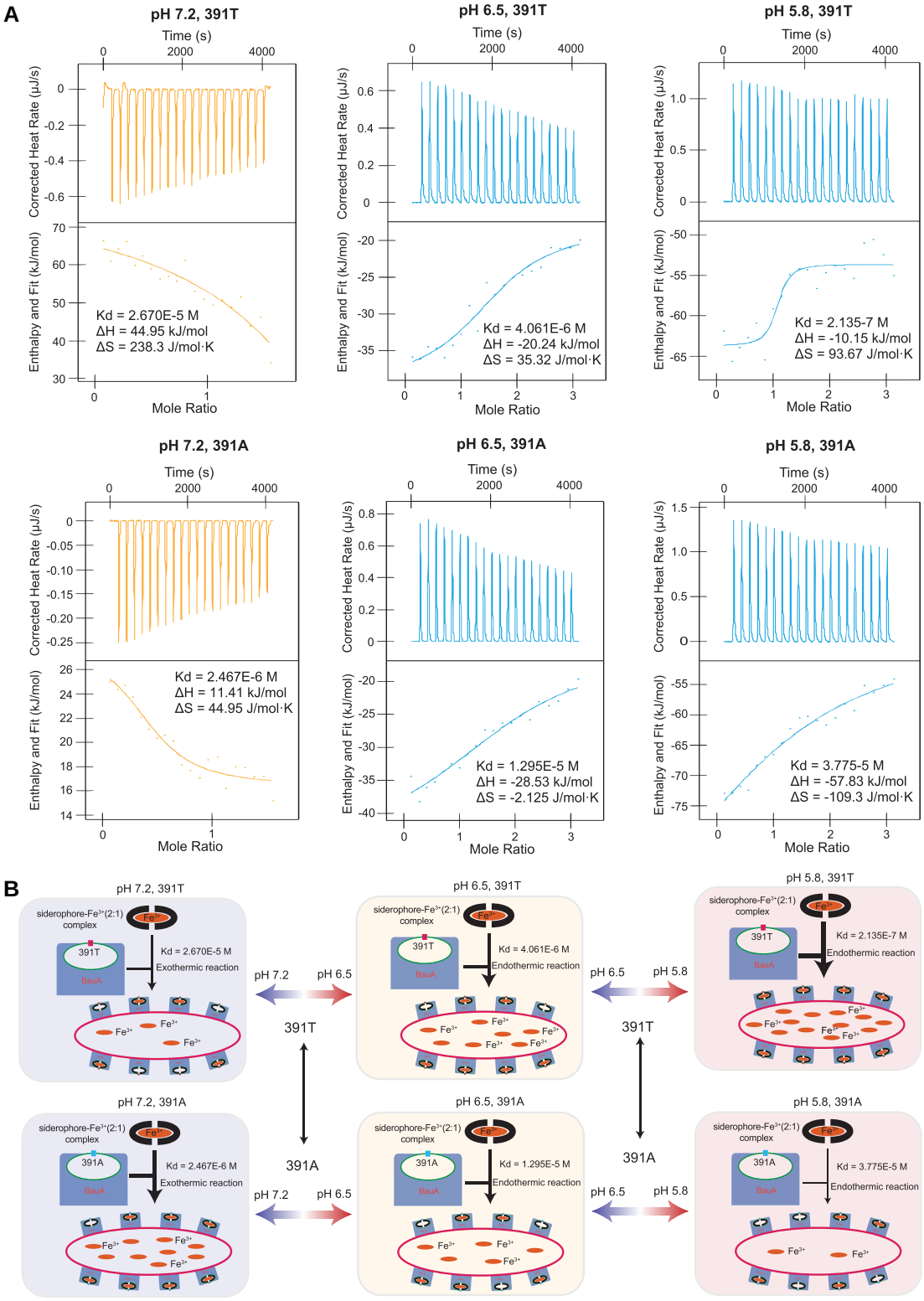

Fig. 4. The mutation between 391A and 39T enhances BauA's binding ability to siderophore at acidic or neutral pH. A) Representative ITC-binding curves for BauA and Fe^{3+}-siderophore (1:2). The test groups included BauA-391A (or BauA-391T) with Fe^{3+}-siderophore (1:2) at pH 5.8, 6.5, or 7.2. The binding data (Kd, ΔH, ΔS) are also shown. B) Proposed paradigm for the role of BauA site 391 in the iron-absorption activity of *Acinetobacter baumannii*. At acidic pH, BauA-391T showed a higher affinity to Fe^{3+}-siderophore (1:2) to acquire more iron ions. In contrast, the mutant with BauA-391A had stronger activity to acquire iron ions in the neutral environment.

compared in an iron-excess or iron-deficient LB medium. In an iron-excess LB medium, there were no significantly differences between the three strains in all the three pH values (Fig. S7A). In an iron-deficient LB medium, the strain with BauA-391A grew significantly faster at pH 7.2; in contrast, the strain with BauA-391T grew significantly better at pH 5.8 or 6.5 ($P < 0.01$, Fig. 5A). Δ*bauA*

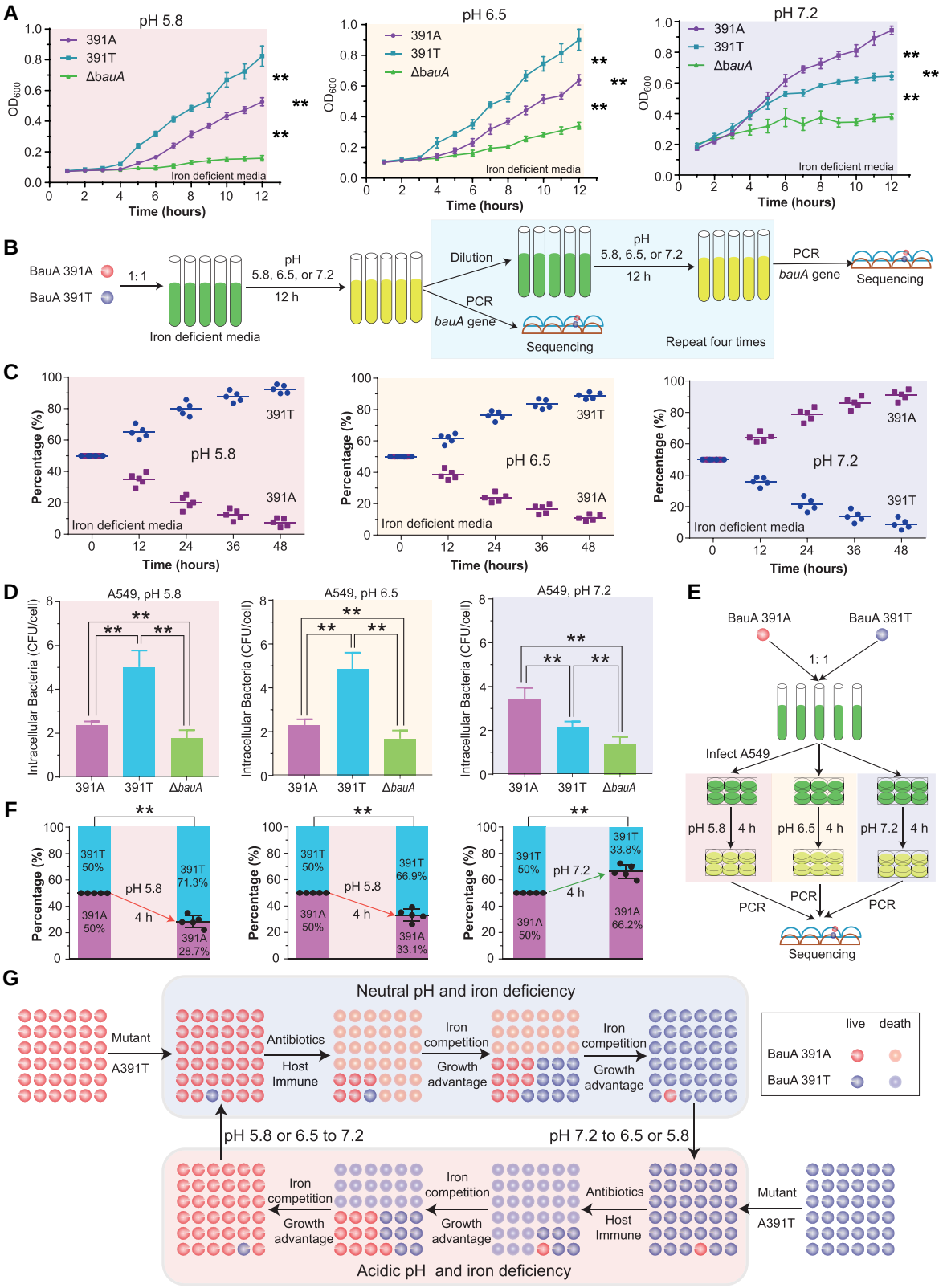

Fig. 5. BauA-391T/A variants are dominant in distinct pH microenvironments. A) The growth curves of the mutants 391A, 391T, and Δ*bauA* of *Acinetobacter. baumannii* strain P5_T08 in LB with 250 μM DIP at pH 5.8, 6.5, or 7.2. $^{**}P < 0.01$. B) Schematic diagram of the growing competition experiment between *A. baumannii* mutants 391A and 391T in an iron-deficient medium. C) The percentage changes of *A. baumannii* mutants in the iron-deficient medium. The two mutants 391A and 391T were mixed in equal proportions and cultured in LB with 200 μM DIP at pH 5.8, 6.5, or 7.2. Subculture and sampling were performed every 12 h. D) The intracellular infection levels of *A. baumannii* mutants 391A, 391T, and Δ*bauA* with A549 alveolar epithelial cells at pH 5.8, 6.5, or 7.2 after 4 h of infection. Intracellular CFU counts were obtained after lysates of Gm-treated A549 cells were plated on LB agar and incubated overnight at 37°C. $^{**}P < 0.01$. E) Schematic diagram of the growing competition experiment between *A. baumannii* mutants 391A and 391T in the infected cells. F) The percentages changes of intracellular *A. baumannii* mutants 391A and 391T in infected A549 cells at pH 5.8, 6.5, or 7.2. The sampling was performed after 4 h of infection. G) Proposed paradigm for the role of BauA mutation site 391 in *A. baumannii* pH adaptability. The opposite conversion of dominant strains between mutations 391T and 391A modulates *A. baumannii* to adapt to different pH environments.

was associated with significantly slower growth compared with the two mutants at neutral and acidic pH ($P < 0.01$). Similar results were observed in the iron-deficient M9 medium (Fig. S7B). Then, the competitive advantage of the strains with BauA-391A or 391T at different pH values was compared in a competitive growth experiment (Fig. 5B). With the successive passage of the mixed strains (1:1), the percentages of BauA-391A mutant gradually increased at pH 7.2 and progressively decreased at pH 5.8 or 6.5 (Fig. 5C). Then, the two mutants of *A. baumannii* were used to infect human lung epithelial cells A549. Plating gentamicin (Gm)-treated cell lysates on an LB medium were used to count the number of intracellular bacteria (Fig. 5D). The number of intracellular bacteria with BauA-391A was significantly higher than that with BauA-391T at pH 7.2 ($P < 0.01$), and significantly lower than that with BauA-391T at pH 5.8 or 6.5 ($P < 0.01$). Similar results were observed in human macrophage cells THP-1 (Fig. S8). Then, the infection with an equal mixture of the two mutants at different pH values was compared in a competitive infection experiment (Fig. 5E). The percentages of intracellular BauA-391T mutants increased from 50 to 71.3% at pH 5.8 (66.9% at pH 6.5); in contrast, they evidently decreased from 50 to 33.8% at pH 7.2 (Fig. 5F). These results indicated that through the A/T mutation at BauA site 391, *A. baumannii* displayed two reversible phases to adapt to distinct pH microenvironments (Fig. 5G). Based on its competitive advantage in iron-deficient environments, such as infected human organs or cells, the BauA-391A mutant was dominant in acidic pH environments, while the 391T mutant was dominant in neutral pH environments. The dynamic equilibrium between two BauA 391 mutants and the microenvironmental pH promotes the persistent survival and infection of *A. baumannii*.

Discussion

Multidrug-resistant *A. baumannii* has become one of the most critical resistant pathogens worldwide. However, there is limited information about its evolution among patients. In this study, 76 isolates (8–12 isolates per patient, spanning 128–188 days) were longitudinally collected from eight patients to investigate the dynamics and mechanisms of within-host evolution using WGS. Longitudinal and high-density continuous sampling helped us to obtain many intermediate isolates, which provided high-resolution insight into the degree of heterogeneity between isolates. Furthermore, 33 isolates were from transmission between four patients, which provides a rare opportunity to compare the evolutionary dynamics of the isogenetic strains across multiple patients. Surprisingly, there was significant variation in the diversification rates, evolutionary routes, and dominant clone types in the strains from the four patients, which revealed the key role of host factors in the within-patient evolution of *A. baumannii*. In addition, we found a high ratio of nonsynonymous relative to synonymous mutations during the within-host evolution of *A. baumannii* in the lungs of these patients (0.91), which is remarkably higher than the reported ratio at the population level of *A. baumannii* (0.18) (10). The mutations were significantly more frequent in protein-coding regions, and multiple genes were identified with parallel mutations in the isolates from different patients. These results strongly suggest that the effect of positive selection is predominant for the within-host evolution of *A. baumannii*.

In this study, we identified multiple within-host evolutionary mechanisms of *A. baumannii* that increase the evolutionary potential to adapt to host environment. An important mechanism used by pathogens is hypermutation, which accelerates the rate of adaptation by increasing the mutation rate. In this study, all of the 12 isolates from patient P2 harbored a mutation P118S in the MutS protein; these isolates were hypermutators, with a 5.1-fold increased mutation rate (P2 vs. other seven patients: 27.5 vs. 5.4 SNPs genome^{-1} y^{-1}), which greatly increased the evolutionary potential to adapt to the novel host environment. Recombination is another factor that can lead to faster diversification of the genome than point mutations alone. In the isolates from patient P1, eight mutations were simultaneously induced by a recombination event, which suggests that recombination is also a strategy to increase the supply of genetic novelty for *A. baumannii*.

In the host, the pathogens such as *A. baumannii* must overcome various challenges, including limited nutrient sources. Hosts have evolved elaborate mechanisms to sequester nutrients, such as iron, a process that is referred to as nutritional immunity (1). *Acinetobacter baumannii* responds to iron starvation by modifying gene expression for genes involved in various processes such as respiration, biofilm formation, and motility, highlighting the importance of iron levels to *A. baumannii* survival and infection (34, 35). In this study, we observed two nutrition-acquisition-related TonB-dependent receptor genes (*bauA* and *BJAB07104_RS00665*) mutations in multiple isolates from different patients, discovering that "nutritional immunity" is an important factor in the within-host evolutionary adaptation of *A. baumannii*. The siderophore receptor gene *bauA* was mutated in multiple isolates from four patients. All of these mutations were at amino acid site 391 in the ligand-binding sites of BauA, with the mutation between A and T. Infected body sites can have a significantly lower pH than healthy tissues (29). *Acinetobacter baumannii* also needs to adapt to different pH values during chronic infection, especially in the acidic microenvironment. This observation is consistent with the discovery of the function of BauA in this study. With two different amino acids (T or A) at site 391, the strains of *A. baumannii* have distinct activities of siderophore-dependent iron acquisition, and reveal growth advantage at acidic or neutral pH, respectively. A comparable mechanism is that of phase variation, which in general refers to a reversible switch between an "all-or-none" (on/off) expressing phase, resulting in variation in the level of expression of one or more proteins between individual cells of a clonal population (36). Similar to the "phase variation," *A. baumannii* with BauA-391A or BauA-391T also reveals two reversible phases to adapt to acidic and neutral environments. Different from the "phase variation," the genetic basis of acidic and neutral phases of *A. baumannii* is the allelic variation in a single residue of BauA protein. It is worth noting that the BauA proteins of *A. baumannii* are divided into three clades based on sequence similarity (Fig. S6). The findings of BauA-391A or -391T in this study were limited to the strains belonging to clade I.

The respiratory tract is the main site of infection and colonization of *A. baumannii* in patients. Airway surface liquid (ASL) is an important microenvironment for *A. baumannii* infection. Many studies reported that the ASL pH varied during pathogen infection in patients (37). One of the studies showed that the respiratory mucus pH was associated with the onset of pneumonia symptoms in the ICU patients (38). In the patients who developed initial colonization and then pneumonia, the pH did not change after colonization, but became acidic with the development of pneumonia. The pH returned to basal levels after recovery from pneumonia. In this study, multiply patients, such as P2 and P5, had recurrent episodes of pneumonia with intermittent fever, and the pneumonia or fever improved with antibiotics. The temperature curves of patients P2 and P5 over time are shown in Fig. S9. These disease presentations suggest that the ASL pH of patients P2 and P5 might

vary with the reduction, disappearance, and reappearance of pneumonia symptoms. To adapt to the changing ASL pH microenvironments, *A. baumannii* displayed two reversible phases through the opposite mutation at BauA site 391. At different pH microenvironments, the proportions of the isolates from the two phases were distinct, as shown in Fig. 5G. However, the clinical strains used in this study were monoclonal, were isolated and randomly collected from the sputum cultures of patients, and thus were mainly representative isolates of the dominant phase. The isolation and culture process used to produce clinical strains have reduced their complexity compared with that of the bacterial community at the site of infection. Therefore, it is necessary to conduct further studies on uncultured clinical infection samples using metagenomes in the future.

In conclusion, our genomic analysis of the longitudinally collected isolates from eight patients revealed the great variation in the rate of diversification and the multiple evolutionary strategies such as hypermutation and recombination, increasing the understanding of the within-host genetic dynamics of *A. baumannii*. In addition, we found multiple adaptive genes and mutation sites related to within-host evolution, which could be targeted to further study the mechanism of *A. baumannii* adaption to host. Importantly, we discovered that an adaptive site of BauA site 391 was an important regulator for *A. baumannii* to adapt to different pH levels, which depicts a model for bacteria adaptation to a constantly changing environment.

Materials and methods

Plasmids, bacteria strains, cells, and reagents

The expression vector pET-28a and pMo130-TelR plasmids were stored in our laboratory. A549 and THP1 cells were also from our laboratory. A HisTrap Fast Flow column (5 mL) was purchased from GE Healthcare (Beijing, China). Taq DNA polymerase and T4 DNA ligase were purchased from New England Biolab. PCR primers were synthesized by GENEWIZ (China). The bacteria genomic DNA extraction kits and plasmid kits were purchased from Qiagen. $^{55}FeCl_3$ solution was from Perkin Elmer. Acinetobactin and preacinetobactin were synthesized by Sks Chem Company. All other chemicals and reagents were obtained from commercial sources and were of the highest purity available.

Patients and bacterial isolates

The patients attending the Fifth Medical Center of PLA General Hospital were closely followed; their sputum samples were tested regularly for the presence of *A. baumannii*, and the identified isolates were stored frozen for further study. Isolation and identification of *A. baumannii* were carried out as previously described (39). A retrospective collection of clinical information about the patients was conducted from the hospital medical records; the collected data included age, admission date, inpatient ward, diagnoses, medications, clinical course, and isolation date.

Antimicrobial susceptibility tests

Clinical strains were grown on blood agar plates, and the minimum inhibitory concentrations of antibiotics were determined for all isolates using BD Phoenix-100 Automated Microbiology System. The antibiotics included amoxicillin/clavulanic acid, amikacin, aztreonam, ceftazidime, chloromycetin (C), CIP, ceftriaxone, cefuroxime, cefazolin, ertapenem, cefepime, fosfomycin, cefoxitin, gentamicin, imipenem, levofloxacin, MEM, minocycline, colistin, nitrofurantoin, moxifloxacin, tobramycin, norfloxacin, ampicillin/sulbactam, SCP, trimethoprim/sulfamethoxazole, tetracycline, piperacillin/tazobactam, and tigecycline. The results were interpreted using Clinical and Laboratory Standards Institute breakpoints.

Whole-genome sequencing

Overnight cultures were grown in LB broth, and genomic DNA was extracted using Wizard Genomic DNA Wizard Genomic DNA Purification Kit (Promega, WI, USA). Paired-end libraries (500 bp fragments) were constructed for all of the strains and were sequenced using an Illumina HiSeq-2000 platform to obtain a 100-bp paired-end read. An average of 9,691,933 reads (range, 5,557,016–17,200,862 reads) were obtained for each of the genomic libraries. In general, we sequenced the isolates with an average genomic coverage of 245-fold (range, 140- to 435-fold). The Illumina short reads were assembled using VELVET (40) and annotated using NCBI's PGAAP pipeline (http://www.ncbi.nlm.nih.gov/genome/annotation_prok/). All of the genomes are available at NCBI under BioProject PRJNA355052.

Bioinformatics analysis

Single-nucleotide polymorphisms between all of the isolated strains were identified by kSNP3 (14) software using the default parameters. A core phylogenetic tree was inferred using SNPs in at least 80% of the genomes and was constructed using the maximum parsimony method in kSNP3 software. The Illumina sequence reads were aligned to the *A. baumannii* reference genome BJAB07104 (39) (accession number: NC_021726; genome size of 3.9 Mb) using *bwa* v0.7.10 (41) software to identify SNPs between strains within each patient. The sites with a mapping quality of <30 and <5 paired-end reads were removed using SAMtools v0.1.19 (42) and homemade Perl script. The remaining SNPs were used to construct the phylogenetic tree via the maximum-likelihood method by RAxML v8.1.6 (43) software (1,000 bootstrap replicates), with the GTR model of nucleotide substitution with the gamma model of rate heterogeneity. Recombination events were investigated using Gubbins (16). Prediction of the hydrophobic transmembrane regions in BauA was done with PRED-TMBB (http://biophysics.biol.uoa.gr/PRED-TMBB/). The webserver was used to find the topology of the loops in addition to localizing the transmembrane strands (15). All the 78 within-host mutations were verified by PCR amplification and Sanger sequencing.

Expression and purification of BauA proteins

To express 6×His fusion proteins, the gene *bauA* (391A and 391T) was cloned into pET-28a and expressed in *Escherichia coli* BL21(DE3). Bacterial culture was grown to an OD_{600} of 0.6 at 37°C in Luria–Bertani (LB) broth; IPTG was added to 0.1 mM, and then cultivated with bacteria with shaking for 20 h at 20°C. Bacteria were collected and crushed by an ultrasonic cell disruptor. Supernatant proteins were purified by Ni-NTA Sepharose in accordance with the manufacturer's protocol and were identified by SDS-PAGE. Finally, target proteins were saved in dialysis MES or HEPES buffer (pH 5.8, 6.5, or 7.2) and stored at −80°C.

Construction of the mutants of *A. baumannii*

To construct the single amino acid mutant of BauA site 391 (A391T, named 391T) or the *bauA* gene deleted mutant (named Δ*bauA*) of *A. baumannii* strain P5_T08, we used a suicide plasmid recombination system (30). Specifically, 1,000 bp homologous regions that were cloned from *A. baumannii* by PCR and SacB gene were inserted into plasmid pMo130-TelR to construct a

recombination vector. With the work of sucrose pressure, the target gene *bauA* was knocked out or replaced. The mutants were obtained and identified by PCR method and Sanger sequencing.

Capsule detection and diameter measurement

The number of capsules was detected using the same method in a previous report (44). The membrane extracts standardized by Bradford assay according to protein concentration were separated on 10% SDS-PAGE. The total proteins were visualized using Coomassie blue stain, and cis-diol sugars were visualized using periodic acid-Schiff stain. Bacterial capsules were detected using the India ink method (22). Briefly, bacterial colonies and India ink were mixed in 0.85% NaCl solution, and the bacteria were observed and photographed under a light microscope (1,000×). The capsule diameters were measured for each isolate using image J software (https://imagej.nih.gov/ij/).

In vitro iron uptake assays

In vitro iron uptake assays were performed as previously described (45). Briefly, acinetobactin and preacinetobactin were synthesized as previously described (46) and dissolved in MOPS buffer. Acinetobactin or preacinetobactin was incubated with $^{55}FeCl_3$ at 37°C for 30 min; 50 µL phosphate sodium buffer was added to remove free iron, and the supernatant was carefully taken after centrifuge. The bacteria were cultured overnight and were collected via centrifugation at 10,000 *g*. The bacterial deposits were washed with cold MOPS three times and were resuspended in MOPS buffer containing 2 g L^{-1} glucose to an OD_{600} of 0.6. The bacteria were preheated at 37°C for 5 min and mixed with acinetobactin or preacinetobactin-$^{55}FeCl_3$ complex. Next, 100 µL aliquots were taken out at 30 min, and we immediately added 1 mL EDTA solution to stop the reaction. The bacteria were centrifuged and washed with 0.85% NaCl, and then 100 µL lysis solution was added for 5 min at 80°C. Finally, the bacterial deposits were incubated with scintillation solution for 12 h in dark and then detected with scintillation analyzer (Perkin Elmer).

Isothermal titration calorimetry

Isothermal titration calorimetry experiments were carried out on an Affinity ITC instrument at 25°C. The BauA-391A and BauA-391T protein concentrations were 20 µM and were dissolved at pH 5.8, 6.5, or 7.2 buffers. Acinetobactin or preacinetobactin was dissolved in the corresponding buffer as proteins with a 200 µM concentration. All binding experiments consisted of the first injection of 2 mL and a 60 s delay. The subsequent 20 injections were of 8 mL at a 200 s interval. The ITC data were analyzed using Launch NanoAnalyze. ITC experiments were done in duplicate.

Bacterial growth and infection of cells at different pH values

The 391A and 391T mutant strains were grown overnight and diluted to a final OD_{600} of 0.01 in M9 or LB medium with 0, 50, or 200 µM DIP adjusted to pH 5.8, 6.5, or 7.2. The bacteria were cultured in 96-well plates with shaking at 37°C, and the OD_{600} value was monitored hourly for 12 h. All of the experiments were performed in triplicate. In the infection experiment, bacterial strains were cultured overnight at 37°C and suspended in PBS; after the cells grew to 90%, we removed the culture medium and replaced it with serum-free DMEM medium (pH 5.8, 6.5, or 7.2). Bacterial cells with a multiplicity of infection of 50 were added to A549 cells or THP-1 cells and incubated at 37°C for 4 h. Then, the infected monolayers were washed three times with PBS. To determine intracellular bacterial persistence, the monolayers were then treated with 2 mL of gentamicin (10 mg mL^{-1} in PBS) for 30 min, the shortest time point that resulted in the death of all bacteria added to the monolayers. The cells were lysed with 0.1% Triton X in PBS; appropriate lysate dilutions were plated on LB agar containing no antibiotics; and the numbers of colony-forming units (CFUs) were recorded after overnight (10 to 12 h) incubation at 37°C. Duplicate assays were done at least three times using fresh samples each time. The data were statistically analyzed using the Student's *t* test. *P*-values <0.05 were considered statistically significant.

The competitive growth and infection experiment

The 391A and 391T mutant strains were grown overnight, equally mixed (1:1), and diluted to a final OD_{600} of 0.01 in LB medium containing 200 µM DIP adjusted to pH 5.8, 6.5, or 7.2. The bacteria were cultured at 37°C for 12 h, and they were divided into two parts. The first part was used to extract genomic DNA. The gene *bauA* was PCR-amplified and sequenced using an Mi-seq platform to detect the percentages of BauA-391T and BauA-391A. The second part was diluted to a final OD_{600} of 0.01, and four successive passages, sampling and sequencing were performed. In the competitive infection experiment, equal mixture of two mutants BauA-391A and BauA-391T was added to A549 cells at pH 5.8, 6.5, or 7.2, and incubated at 37°C for 4 h. The infected cells were lysed after gentamicin treatment; gene *bauA* was PCR-amplified and sequenced to detect the percentages of BauA-391T and BauA-391A.

Statistics

Data were described with means and standard deviation. Dichotomous variables were described with percentages. The quantitative data were compared using the paired Student's *t* test. *P*-values <0.05 were considered statistically significant, and all *P*-values were two-tailed. We conducted all statistical analyses using GraphPad Prism version 6.01.

Supplementary material

Supplementary material is available at *PNAS Nexus* online.

Funding

This work was supported by National Natural Science Foundation of China (82072251), National Key Basic Research Program (973) of China (2015CB554202), and Beijing Nova Program (Z181100006218111).

Author contributions

H.W. and T.L. designed the study. C.B., F.Q., and B.L. provided the isolates and patient information. N.N. and X.L. extracted DNA of the isolates. X.L. conducted the genome assembly, analysis, and data deposition. L.Z., Z.L., D.L., H.G., X.Y., and Y.H. participated in data analysis and discussion. F.C., T.L., and N.N. performed the experiment about BauA and Wzc. The manuscript was written by T.L. and X.L., and modified by D.L. and H.W. All authors read and approved the final manuscript.

Data availability

This Whole Genome Shotgun project has been deposited in GenBank under BioProject PRJNA355052. The genome sequences and annotation were available at the NCBI (https://www.ncbi.nlm.nih.gov/bioproject/PRJNA355052).

References

1 Harding CM, Hennon SW, Feldman MF. 2018. Uncovering the mechanisms of *Acinetobacter baumannii* virulence. *Nat Rev Microbiol*. 16(2):91–102.
2 Dijkshoorn L, Nemec A, Seifert H. 2007. An increasing threat in hospitals: multidrug-resistant *Acinetobacter baumannii*. *Nat Rev Microbiol*. 5(12):939–951.
3 Vázquez-López R, *et al.* 2020. *Acinetobacter baumannii* resistance: a real challenge for clinicians. *Antibiotics*. 9(4):205.
4 Didelot X, Walker AS, Peto TE, Crook DW, Wilson DJ. 2016. Within-host evolution of bacterial pathogens. *Nat Rev Microbiol*. 14(3):150–162.
5 Marvig RL, Sommer LM, Molin S, Johansen HK. 2015. Convergent evolution and adaptation of *Pseudomonas aeruginosa* within patients with cystic fibrosis. *Nat Genet*. 47(1):57–64.
6 Lieberman TD, *et al.* 2011. Parallel bacterial evolution within multiple patients identifies candidate pathogenicity genes. *Nat Genet*. 43(12):1275–1280.
7 Fitzpatrick MA, Ozer EA, Hauser AR. 2016. Utility of whole-genome sequencing in characterizing Acinetobacter epidemiology and analyzing hospital outbreaks. *J Clin Microbiol*. 54(3):593–612.
8 Kanamori H, *et al.* 2015. Next-generation sequencing and comparative analysis of sequential outbreaks caused by multidrug-resistant *Acinetobacter baumannii* at a large academic burn center. *Antimicrob Agents Chemother*. 60(3):1249–1257.
9 Wen H, *et al.* 2014. Population dynamics of an *Acinetobacter baumannii* clonal complex during colonization of patients. *J Clin Microbiol*. 52(9):3200–3208.
10 Wright MS, Iovleva A, Jacobs MR, Bonomo RA, Adams MD. 2016. Genome dynamics of multidrug-resistant *Acinetobacter baumannii* during infection and treatment. *Genome Med*. 8(1):26.
11 Wright MS, *et al.* 2014. New insights into dissemination and variation of the health care-associated pathogen *Acinetobacter baumannii* from genomic analysis. *mBio*. 5(1):e00963-00913.
12 Snitkin ES, *et al.* 2012. Tracking a hospital outbreak of carbapenem-resistant *Klebsiella pneumoniae* with whole-genome sequencing. *Sci Transl Med*. 4(148):148ra116.
13 Hornsey M, *et al.* 2011. Whole-genome comparison of two *Acinetobacter baumannii* isolates from a single patient, where resistance developed during tigecycline therapy. *J Antimicrob Chemother*. 66(7):1499–1503.
14 Gardner SN, Slezak T, Hall BG. 2015. kSNP3.0: SNP detection and phylogenetic analysis of genomes without genome alignment or reference genome. *Bioinformatics*. 31(17):2877–2878.
15 Antunes LC, Visca P, Towner KJ. 2014. *Acinetobacter baumannii*: evolution of a global pathogen. *Pathog Dis*. 71(3):292–301.
16 Croucher NJ, *et al.* 2015. Rapid phylogenetic analysis of large samples of recombinant bacterial whole genome sequences using Gubbins. *Nucleic Acids Res*. 43(3):e15.
17 Snitkin ES, *et al.* 2011. Genome-wide recombination drives diversification of epidemic strains of *Acinetobacter baumannii*. *Proc Natl Acad Sci USA*. 108(33):13758–13763.
18 Azarian T, *et al.* 2016. Intrahost evolution of methicillin-resistant *Staphylococcus aureus* USA300 among individuals with reoccurring skin and soft-tissue infections. *J Infect Dis*. 214(6):895–905.
19 Oliver A, Mena A. 2010. Bacterial hypermutation in cystic fibrosis, not only for antibiotic resistance. *Clin Microbiol Infect*. 16(7):798–808.
20 Didelot X, *et al.* 2012. Microevolutionary analysis of *Clostridium difficile* genomes to investigate transmission. *Genome Biol*. 13-(12):R118.
21 Russo TA, *et al.* 2010. The K1 capsular polysaccharide of *Acinetobacter baumannii* strain 307-0294 is a major virulence factor. *Infect Immun*. 78(9):3993–4000.
22 Hua X, *et al.* 2017. Evolution of *Acinetobacter baumannii* in vivo: international clone II, more resistance to ceftazidime, mutation in ptk. *Front Microbiol*. 8:1256.
23 Talyansky Y, *et al.* 2021. Capsule carbohydrate structure determines virulence in *Acinetobacter baumannii*. *PLoS Pathog*. 17(2):e1009291.
24 Akoolo L, Pires S, Kim J, Parker D. 2022. The capsule of *Acinetobacter baumannii* protects against the innate immune response. *J Innate Immun*. 14(5):543–554.
25 Damier-Piolle L, Magnet S, Brémont S, Lambert T, Courvalin P. 2008. AdeIJK, a resistance-nodulation-cell division pump effluxing multiple antibiotics in *Acinetobacter baumannii*. *Antimicrob Agents Chemother*. 52(2):557–562.
26 Gallarato LA, *et al.* 2014. Exopolyphosphatase of *Pseudomonas aeruginosa* is essential for the production of virulence factors, and its expression is controlled by NtrC and PhoB acting at two interspaced promoters. *Microbiology*. 160(Pt 2):406–417.
27 Zimbler DL, *et al.* 2009. Iron acquisition functions expressed by the human pathogen *Acinetobacter baumannii*. *Biometals*. 22(1):23–32.
28 Shapiro JA, Wencewicz TA. 2017. Structure-function studies of acinetobactin analogs. *Metallomics*. 9(5):463–470.
29 Higgins PG, Stubbings W, Wisplinghoff H, Seifert H. 2010. Activity of the investigational fluoroquinolone finafloxacin against ciprofloxacin-sensitive and -resistant *Acinetobacter baumannii* isolates. *Antimicrob Agents Chemother*. 54(4):1613–1615.
30 Amin IM, *et al.* 2013. A method for generating marker-less gene deletions in multidrug-resistant *Acinetobacter baumannii*. *BMC Microbiol*. 13:158.
31 McKay SL, *et al.* 2022. Molecular epidemiology of carbapenem-resistant *Acinetobacter baumannii* in the United States, 2013–2017. *Microbial Drug Resistance*. 28(6):645–653.
32 Chen T, *et al.* 2021. *Acinetobacter baumannii* strains isolated from cerebrospinal fluid (CSF) and bloodstream analysed by cgMLST: the dominance of clonal complex CC92 in CSF infections. *Int J Antimicrob Agents*. 58(4):106404.
33 Bian X, *et al.* 2021. Epidemiological and genomic characteristics of *Acinetobacter baumannii* from different infection sites using comparative genomics. *BMC Genomics*. 22(1):530.
34 Eijkelkamp BA, Hassan KA, Paulsen IT, Brown MH. 2011. Investigation of the human pathogen *Acinetobacter baumannii* under iron limiting conditions. *BMC Genomics*. 12:126.
35 Nwugo CC, Gaddy JA, Zimbler DL, Actis LA. 2011. Deciphering the iron response in *Acinetobacter baumannii*: a proteomics approach. *J Proteomics*. 74(1):44–58.
36 van der Woude MW, Bäumler AJ. 2004. Phase and antigenic variation in bacteria. *Clin Microbiol Rev*. 17(3):581–611.
37 Zajac M, Dreano E, Edwards A, Planelles G, Sermet-Gaudelus I. 2021. Airway surface liquid pH regulation in airway epithelium current understandings and gaps in knowledge. *Int J Mol Sci*. 22(7):3384.

38 Karnad DR, Mhaisekar DG, Moralwar KV. 1990. Respiratory mucus pH in tracheostomized intensive care unit patients: effects of colonization and pneumonia. *Crit Care Med*. 18(7):699–701.
39 Zhu L, *et al*. 2013. Complete genome analysis of three *Acinetobacter baumannii* clinical isolates in China for insight into the diversification of drug resistance elements. *PLoS One*. 8(6):e66584.
40 Zerbino DR, Birney E. 2008. Velvet: algorithms for de novo short read assembly using de Bruijn graphs. *Genome Res*. 18(5):821–829.
41 Li H, Durbin R. 2009. Fast and accurate short read alignment with Burrows-Wheeler transform. *Bioinformatics*. 25(14):1754–1760.
42 Li H, *et al*. 2009. The sequence alignment/map format and SAMtools. *Bioinformatics*. 25(16):2078–2079.
43 Stamatakis A. 2006. RAxML-VI-HPC: maximum likelihood-based phylogenetic analyses with thousands of taxa and mixed models. *Bioinformatics*. 22(21):2688–2690.
44 Lees-Miller RG, *et al*. 2013. A common pathway for O-linked protein-glycosylation and synthesis of capsule in *Acinetobacter baumannii*. *Mol Microbiol*. 89(5):816–830.
45 Barnard TJ, Watson ME Jr, McIntosh MA. 2001. Mutations in the *Escherichia coli* receptor FepA reveal residues involved in ligand binding and transport. *Mol Microbiol*. 41(3): 527–536.
46 Takeuchi Y, *et al*. 2010. Synthesis of acinetobactin. *Chem Pharm Bull*. 58(11):1552–1553.